Received: 13 December 2021 | Revised: 6 March 2022 | Accepted: 30 March 2022

DOI: 10.1002/er.7951

RESEARCH ARTICLE

INTERNATIONAL JOURNAL OF ENERGY RESEARCH WILEY

Design and analysis of an iodine-sulfur thermochemical cycle-based hydrogen production system with an internal heat exchange network

Qi Wang | **Rafael Macián-Juan**

Chair of Nuclear Technology, Technical University of Munich (TUM), Garching, Germany

Correspondence
Qi Wang, Chair of Nuclear Technology, Technical University of Munich (TUM), 85748, Garching, Germany.
Email: qi.wang@tum.de

Funding information
China Scholarship Council, Grant/Award Number: 202006280024; Technische Universität München

Summary

The iodine-sulfur (I-S) cycle is one of the most promising thermochemical cycles to produce carbon-free hydrogen on a large scale. The employment of an efficient internal heat exchange network is very essential for the efficiency improvement of the I-S cycle, however, detailed research on this topic is seldomly reported. To enrich the existing research content, an I-S cycle-based hydrogen production system with an internal heat exchange network is proposed in this paper using Aspen Plus. The internal heat exchange network is designed by following the energy cascade utilization principle, and three sets of different heat transfer constraints corresponding to different temperature zones are imposed in the design process. The simulation results show that for the proposed I-S system, more than half of the system energy consumption is used by the distillation processes of two acid solutions, and more than 40% of the system energy consumption is used by the HI concentration and distillation process. Using the internal heat exchange network, about 422 kJ of waste heat (for 1 mol of hydrogen production) can be recovered and the system thermal efficiency is improved by about 4.9%. In addition, an efficiency improvement of about 11.8% can be achieved when the waste heat from the condensers of two distillation columns is completely recovered. In general, the thermal efficiency of the proposed I-S system is estimated to be in the range of 15.8% to 49.8%, and after adopting several common waste heat recovery measures, the system can achieve a promising thermal efficiency of approximately 36.7%.

KEYWORDS

efficiency improvement, hydrogen production, internal heat exchange network, iodine-sulfur thermochemical cycle, system design

1 | INTRODUCTION

Nowadays, the exploitation and utilization of clean energy have received growing attention from many countries and regions since it is viewed as the most effective approach to reducing fossil fuel consumption and carbon emissions. As an important clean energy carrier, hydrogen has a number of advantages including environmentally friendly, renewable, abundant reserves, high heating value, easy storability, and transportability, which conversely make it a very important raw material used widely in many industrial sectors such as natural gas synthesis, petrochemical industry, metallurgy, fertilizer production, and so on. According to a report issued by Hydrogen Council in 2017, approximately 18% of the world's energy consumption in 2050 will be supplied by hydrogen.[1] As a result, hydrogen is today enjoying an unprecedented development momentum.[2]

Since hydrogen is the lightest element and can overcome the earth's gravity easily,[3] free hydrogen molecules do not exist in nature and must be produced from hydrogen-containing compounds such as hydrocarbons and water. Currently, nearly 96% of hydrogen is extracted from hydrocarbons (in more detail, 48% from natural gas reforming, 30% from coal gasification, and 18% from oil cracking),[4] and only about 4% of hydrogen is produced from water by electrolysis.[5] These processes are acceptable for applications in the near and medium term due to their high technological maturity and commercial viability. However, from the perspective of long-term development, these methods are no longer feasible because a huge amount of fossil fuels and electricity are consumed during the hydrogen production process, causing significant carbon emissions.[6] Therefore, several advanced thermochemical water-splitting cycles including the iodine-sulfur (I-S) cycle[7] and the copper-chlorine (Cu-Cl) cycle[8] are proposed and are currently being studied actively by many researchers as these cycles are very promising to achieve the large-scale carbon-free hydrogen production when they are coupled with a solar heliostat system[9] or a generation IV nuclear reactor system.[10]

The I-S cycle developed by General Atomics in the 1970s is one of the most famous thermochemical water-splitting cycles and has been widely studied by many countries,[11] such as France,[12] America,[13] Japan,[14] China,[15] and Korea. Figure 1 shows a schematic diagram of the I-S cycle. It can be seen that the net reaction of the three basic chemical reactions in the I-S cycle is equal to splitting water (H_2O) into oxygen (O_2) and hydrogen (H_2) with the supply of thermal energy.[17] Up to now, there are some experimental and simulation studies on the three basic chemical reactions that have been carried out. For instance, Zhu et al[18] experimentally investigated the occurrence of Bunsen side reactions and evaluated the effects of three key operating parameters including the I_2 content, H_2O content, and reaction temperature on the side reactions. Park et al[19] conducted a simulation and experimental study on the H_2SO_4 decomposition process of the I-S cycle. They tailored a proper electrolyte thermodynamic model for the H_2SO_4-H_2O system and found that the process simulation results were in good agreement with the measured experimental data. Gao et al[20] investigated the H_2SO_4 decomposition reaction using ANSYS FLUENT software, and the effects of two different catalyst shapes on the H_2SO_4 decomposition fraction were analyzed. The simulation results showed that the square catalyst could achieve a better catalytic performance than the circular catalyst. In addition, Guo et al[21] performed a simulation study on the energy-intensive HI distillation process, and the obtained results showed that the distillate rate at the minimum heat duty per unit HI throughput increased with the increase of the operating pressure, regardless of the feed concentration.

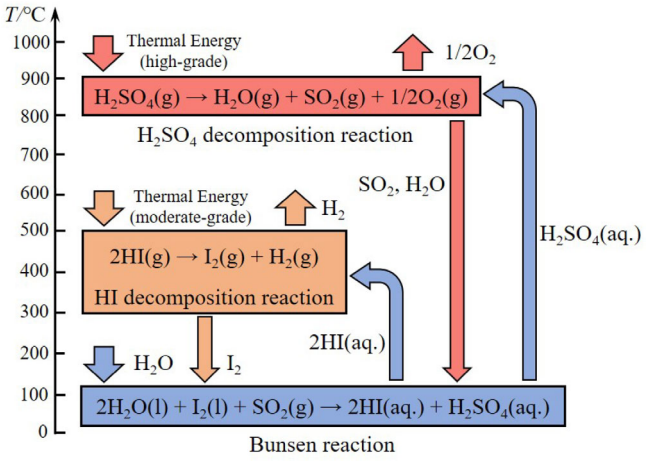

FIGURE 1 A schematic diagram of the I-S cycle (Modified from Reference 16)

For the research on the whole I-S system, there are also some experimental and simulation studies that have been conducted so far. For example, a laboratory-scale I-S facility with a hydrogen production capacity of 50 normal liters per hour (NL/h) was designed and built-in Japan from 1999 to 2005, and 1 week of continuous hydrogen production at a rate of about 30 NL/h was successfully achieved by this facility in 2004.[22] In China, a bench-scale I-S facility with a hydrogen production capacity of 100 NL/h was constructed in 2014, and a successful operation of 60 hours at a hydrogen production rate of 60 NL/h was realized by this facility.[23] Kasahara et al[24] proposed a novel I-S process flowsheet for large-scale highly efficient hydrogen production, and they found that the proposed I-S system could achieve high

thermal efficiency of 50.2%. Park et al[25] proposed a modified I-S cycle driven by a steam boiler heat source and compared this modified cycle with the original cycle from the perspectives of thermodynamic, techno-economic, socio-economic, and risk. The analysis results showed that the modified cycle could achieve a better performance than the original cycle in all aspects. Ying et al[26] proposed an improved I-S cycle integrated with HI electrolysis reaction. The simulation results proved that the improved I-S cycle could achieve a theoretical thermal efficiency of 25% to 42%, which is dependent on the performance of the added internal heat exchange network. By conducting a simple heat transfer analysis, a preliminary internal heat exchange network was designed by them, and a feasible cycle thermal efficiency of 33.3% was finally reached. Besides, Ying et al[7] also developed another novel I-S cycle assembled with HI-I_2-H_2O electrolysis process, and based on the same method, an initial internal heat exchange network was designed and a cycle thermal efficiency of 19.2% was achieved. Recently, Juárez-Martínez et al[27] specially designed an internal heat exchange network for optimizing the energy use of the I-S cycle, by adopting the minimum heat transfer temperature difference constraint. The simulation results indicated that the average energy efficiency of the I-S cycle was improved by about 10% after using the internal heat exchange network.

From the above literature review, it can be seen that the application of an efficient internal heat exchange network is a very important way to improve the efficiency of the I-S cycle, but detailed research on this topic is seldomly reported. More specifically, the internal heat exchange network was preliminarily designed by conducting a simple heat transfer analysis or adopting the minimum heat transfer temperature difference constraint. Since the I-S cycle has a very large operating temperature range (as shown in Figure 1, the operating temperature range of the I-Scycle can vary from 20°C to 900°C), in this situation, it is very necessary to apply different heat transfer constraints to different temperature zones. However, to the best of the authors' knowledge, research on this subject has not been conducted until now. In addition, the previous studies on the design of an internal heat exchange network only considered the terminal heat transfer condition of the heat exchanger while the internal heat transfer process of the heat exchanger was not analyzed. Since most of the streams in the I-S cycle are multicomponent mixtures and some of them undergo phase change during the heating or cooling process, their temperature evolution profiles are likely to be some curved lines or broken lines. At this time, the complete heat transfer process inside the heat exchanger should be studied in detail to avoid the unreasonable intersection of temperature curves of the cold and hot fluids. In this case, the pinch point temperature difference constraint should also be included in the design process. Thus, it is very essential to further refine the design process of the internal heat exchange network, which promotes us to carry out such a study.

In this paper, an I-S cycle-based hydrogen production system with an internal heat exchange network is developed and analyzed using Aspen Plus software. The internal heat exchange network is designed based on the energy cascade utilization principle, and in particular, three sets of different heat transfer constraints corresponding to different temperature zones have been imposed in the design process. In general, this work is helpful for enriching the existing research on the design of the internal heat exchange network, and the proposed I-S system is promising to be used for green hydrogen production in the near future.

2 | SYSTEM DESCRIPTION AND PARAMETER SETTING

2.1 | System description

The schematic process flowsheet of the proposed I-S hydrogen production system without an internal heat exchange network is shown in Figure 2. It is seen that the I-S system consists of three sections which are respectively the Bunsen section, the H_2SO_4 concentration and decomposition section, and the HI concentration and decomposition section.

In the Bunsen section, the H_2O from ambient conditions (25°C and 1 atm) is pressurized and heated before being sent to the BUNSEN reactor where it reacts with the recycled materials including SO_2 and I_2, and generates two immiscible acid solutions (ie, H_2SO_4 and HI solutions) according to the following chemical equation[26]:

$$(1+m)I_2 + SO_2 + (2+n_1+n_2)H_2O \rightarrow (H_2SO_4 + n_1H_2O) + (2HI + mI_2 + n_2H_2O). \quad (1)$$

After completing the Bunsen reaction, the generated H_2SO_4 and HI solutions will be successively separated and purified before being sent to their respective concentration and decomposition sections for O_2 and H_2 production.

In the H_2SO_4 concentration and decomposition section, the gaseous H_2SO_4 is decomposed into H_2O, SO_2, and O_2 by undergoing the following two sub-chemical reactions:

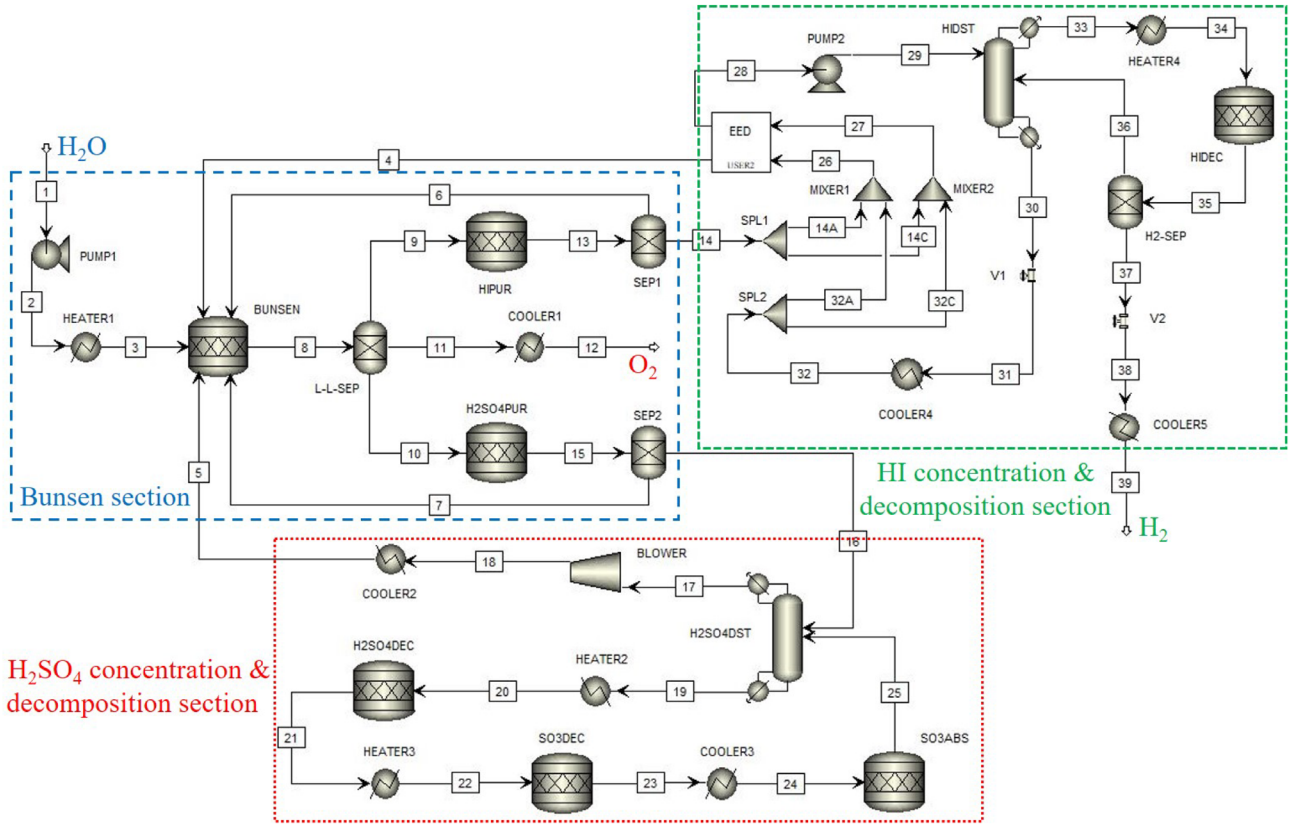

FIGURE 2 Schematic process flowsheet of the proposed I-S hydrogen production system without an internal heat exchange network

$$H_2SO_4 \rightarrow SO_3 + H_2O, \quad (2)$$

$$SO_3 \rightarrow SO_2 + 0.5O_2. \quad (3)$$

In this work, the above two sub-chemical reactions are considered to occur in two independent reactors (ie, H2SO4DEC and SO3DEC, see Figure 2).[26] After completing the SO_3 decomposition reaction, the products are sent to the SO3 absorber (SO_3ABS) where the undecomposed SO_3 will react with H_2O and generate H_2SO_4 again. The generated H_2SO_4 is sent back to the H_2SO_4 distillation column (H_2SO_4DST) for recycling, as shown in Figure 2.

It is well-known that the HI-I_2-H_2O phase obtained from the Bunsen section is a ternary pseudo-azeotropic mixture, and the conventional distillation method is unable to extract high-purity HI from this three-phase mixture.[16] In this work, the electro-electrodialysis (EED) and distillation methods are adopted to solve this problem. As shown in Figure 2, the purified HI solution (Stream 14) is first sent to the EED unit to produce the over-azeotropic HI solution (Stream 28), and then, the obtained over-azeotropic HI solution is pumped to the HI distillation column (HIDST) for extracting high-purity HI. Finally, the top distillate (ie, high-purity HI) is decomposed into H_2 and I_2 in the HI decomposition reactor (HIDEC), and the bottom product is incorporated into the EED cell for reducing the energy consumption of the system, as illustrated in Figure 2.

2.2 | Parameter setting

Taking the H_2 production rate of 1 mol/s as a simulation case, the main operating parameters of the I-S cycle are summarized in Table 1. In the actual operation process, the initial feed conditions of the Bunsen reaction (or the molar ratio of I_2 and H_2O in Bunsen reaction, namely the coefficients m and n in Equation [1]) should be determined carefully because it affects not only the phase compositions of the Bunsen products but also the material flow and energy consumption of the entire I-S system. In this work, to verify the reliability of simulation results, the phase compositions of the Bunsen products are directly specified by referring to the experimental study of Guo et al.[28] In more detail, the $H_2O/H_2SO_4/HI/I_2/O_2$ mixture (Stream 8) with the molar ratio of 34.028/1.656/5.859/7.048/0.5 (ie, molar fraction of 0.69/0.03/0.12/0.14/0.01[28]) is assumed to be obtained at the BUNSEN reactor outlet. Further, when this mixture

TABLE 1 The I-S cycle's main operating parameters (H_2 production rate of 1 mol/s)

Sections	Components	Main operating parameters
Bunsen section	BUNSEN	SO_2 conversion rate: 100%[28]; $T = 353$ K[28]; $p = 0.5$ MPa Molar flow rate of the Bunsen products (mol/s): $H_2O/H_2SO_4/HI/I_2/O_2 = 34.028/1.656/5.859/7.048/0.5$ (molar fraction: 0.69/0.03/0.12/0.14/0.01[28])
	L-L-SEP	Molar flow rate of the H_2SO_4 phase (mol/s): $H_2O/H_2SO_4/HI/I_2 = 4.318/1.091/0.182/0.068$ (molar fraction: 0.76/0.19/0.03/0.01[28])
	HIPUR	H_2SO_4 conversion rate: 100%[26]; $T = 353$ K; $p = 0.5$ MPa
	H2SO4PUR	HI conversion rate: 100%[26]; $T = 353$ K; $p = 0.5$ MPa
H_2SO_4 concentration and decomposition section	H2SO4DST	Number of stages: 5[28]; reflux ratio: 1[28]; distillate rate: 6.056 mol/s; feed location: stage 3[28]; $p = 1$ atm[28]
	H2SO4DEC	H_2SO_4 conversion rate: 100%; $T = 773.15$ K; $p = 1$ atm
	SO3DEC	SO_3 conversion rate: 78%[28]; $T = 1123.15$ K[28]; $p = 1$ atm[28]
	SO3ABS	SO_3 absorption rate: 100%[26]; $T = 473.15$ K[26]; $p = 1$ atm[26]
HI concentration and decomposition section	EED cell	Molar ratio of the cathode outlet stream: $HI:I_2:H_2O = 0.182:0.05:0.768$ (HI molality of the cathode outlet stream: 13.17 mol/kg·H_2O[24]); proton transport number: $t_+ = 1$[24]; electro-osmosis coefficient: $\beta = 1$[24]; $T = 353$ K; $p = 0.5$ MPa
	HIDST	Number of stages: 7[29]; reflux ratio: 3; distillate rate: 5 mol/s; feed location: stage 4; $p = 1.17$ MPa[29,30]
	HIDEC	HI conversion rate: 40%[31]; $T = 723$ K[29,30]; $p = 1.17$ MPa[29,30]

is fed to the liquid-liquid separator (L-L-SEP), the $H_2O/H_2SO_4/HI/I_2$ stream (Stream 10) with the molar ratio of 4.318/1.091/0.182/0.068 (ie, molar fraction of 0.76/0.19/0.03/0.01[28]) can be obtained at the H_2SO_4 phase outlet of L-L-SEP. Besides, to simplify the modeling process, the assumption of a 100% conversion rate for purification processes is adopted in this work based on Reference 26.

As mentioned earlier, the H_2SO_4 decomposition process is divided into two sub-reactions which are respectively occurring in the H2SO4DEC and SO3DEC. In this work, the H_2SO_4 is decomposed into SO_3 and H_2O at 773.15 K (500°C) with a 100% conversion rate, and SO_3 is catalytically decomposed into SO_2 and O_2 at 1123.15 K (850°C) with 78% conversion rate (In Reference 28, the H_2SO_4 is directly decomposed into SO_2, O_2, and H_2O at 1123 K with 78% conversion rate). In addition, it should be noted that the H_2 membrane separator is used in this study to improve the conversion rate of HI decomposition. According to References 24, 29, 30, the HI conversion rate can reach 44% to 50% when the membrane separation technology is applied. However, considering the current technology uncertainty and potential operating risks, this value is conservatively set to 40%.[31] Lastly, it should be emphasized that in Figure 2, all the chemical reactors (such as BUNSEN, HIPUR, H2SO4PUR, H2SO4DEC, etc.) are the type of Stochiometric Reactor, and all the separation components (such as L-L-SEP, SEP1, SEP2, H2-SEP, etc.) are the ordinary component separators.

3 | MATHEMATICAL MODELING AND METHODOLOGY

3.1 | Mathematical modeling

Models of the system components other than the EED cell have already been embedded in Aspen Plus software, so the only mission left is to construct the mathematical model of the EED cell. In this work, the user-defined module of Aspen Plus, USER2, is employed to simulate the EED unit (see Figure 2), and its mathematical model is created and executed by developing an external EXCEL program.

Figure 3 presents a schematic diagram of the EED cell's working principle. It is seen that the EED cell is divided into two compartments (ie, anode and cathode) via a membrane, and in the two compartments, a pair of opposite electrochemical reactions proceeds. In more detail, the iodine ions are oxidized into iodine molecules at the anode, while the iodine molecules are reduced into iodine ions at the cathode. During this process, some hydrogen ions (H^+) will penetrate through the membrane from anode to cathode in the form of hydronium ions (H_3O^+), and conversely, some iodide ions will

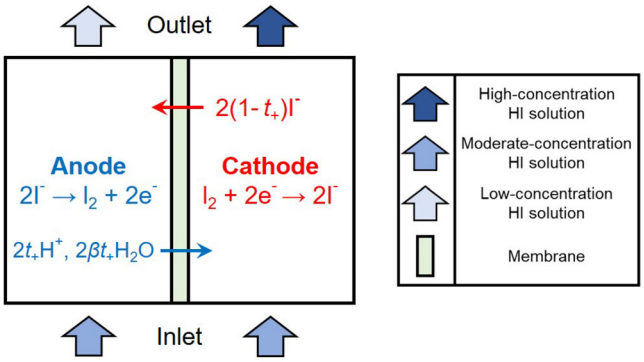

FIGURE 3 Schematic diagram of the EED cell's working principle

penetrate through the membrane from cathode to anode. Eventually, the solution with a high HI concentration is obtained at the cathode outlet, and the diluted solution with a low HI concentration is generated at the anode outlet.

Based on the mass conservation law and Faraday's second law, the EED cell's inlet and outlet equations regarding the electrode's total molar flow rate and each composition's molar flow rate can be respectively expressed by:

$$\begin{cases} n_{\text{out}}^{ca} = n_{\text{in}}^{ca} + \dfrac{(2t_+ - 1 + 2\beta t_+)}{2\text{F}} I \\ n_{\text{out}}^{an} = n_{\text{in}}^{an} - \dfrac{(2t_+ - 1 + 2\beta t_+)}{2\text{F}} I \end{cases}, \tag{4}$$

$$\begin{cases} n_{\text{out,HI}}^{ca} = n_{\text{in,HI}}^{ca} + \dfrac{t_+ I}{\text{F}} \\ n_{\text{out,HI}}^{an} = n_{\text{in,HI}}^{an} - \dfrac{t_+ I}{\text{F}} \\ n_{\text{out,I}_2}^{ca} = n_{\text{in,I}_2}^{ca} - \dfrac{I}{2\text{F}} \\ n_{\text{out,I}_2}^{an} = n_{\text{in,I}_2}^{an} + \dfrac{I}{2\text{F}} \\ n_{\text{out,H}_2\text{O}}^{ca} = n_{\text{in,H}_2\text{O}}^{ca} + \dfrac{\beta t_+ I}{\text{F}} \\ n_{\text{out,H}_2\text{O}}^{an} = n_{\text{in,H}_2\text{O}}^{an} - \dfrac{\beta t_+ I}{\text{F}} \end{cases}, \tag{5}$$

where superscripts *ca* and *an* denote cathode and anode, respectively; subscripts in and out represent inlet and outlet, respectively; symbols n, t_+, β, F, and I are molar flow rate, proton transport number, electro-osmosis coefficient, Faraday constant (96 485 C/mol), and current, respectively.

The electrical power consumption of the EED cell, $E_{\text{con,EED}}$, can be calculated by:

$$E_{\text{con,EED}} = U \cdot I = \left(U_{\text{eq}} + U_{\text{mem}}\right) \cdot I, \tag{6}$$

where terms U_{eq} and U_{mem} respectively represent the equilibrium potential difference between two electrodes and the membrane potential drop. According to References 16, 32, the equilibrium potential difference, U_{eq}, can be calculated by:

$$U_{\text{eq}} = -4.7 \times 10^{-6} \cdot T \cdot \exp\left(\frac{1.6 \times 10^3}{T}\right) \times \ln\left[\left(\frac{\chi_{\text{mn,HI}}^{an}}{\chi_{\text{mn,HI}}^{ca}}\right)^2 \left(\frac{\chi_{\text{mn,I}_2}^{an}}{\chi_{\text{mn,I}_2}^{ca}}\right)^{-\frac{1}{2}}\right], \tag{7}$$

where the term $\chi_{\text{mn},i}$ is the mean mole fraction of composition i at the inlet and outlet of the electrode.

According to Reference 16, the membrane potential drop, U_{mem}, can be calculated by:

$$U_{\text{mem}} = \left[-10.91 \times \left(\chi_{\text{mn,HI}}^{ca} + \chi_{\text{mn,HI}}^{an}\right) + 76.74 \times \left(\chi_{\text{mn,I}_2}^{ca} + \chi_{\text{mn,I}_2}^{an}\right)\right] \times (T - 273.15)^{-1.059}. \tag{8}$$

Thus, the thermal efficiency of the I-S system, $\eta_{\text{I-S}}$, can be calculated by:

$$\eta_{\text{I-S}} = \frac{n_{\text{H}_2} \cdot \text{HHV}_{\text{H}_2}}{Q_{\text{con,I-S}} + \frac{E_{\text{con,I-S}}}{\eta_{\text{ele}}}}, \tag{9}$$

where terms $Q_{\text{con,I-S}}$, $E_{\text{con,I-S}}$, and η_{ele} respectively represent the I-S system's thermal power consumption, electrical power consumption, and the electricity generation efficiency (set as 45%[26]). Since most of the existing studies used the hydrogen's high heating value (HHV_{H2}, set as 285.83 kJ/mol[11]) to estimate the thermal efficiency of the I-S cycle, this value is also adopted in this work for the convenience of conducting the comparison of the efficiency estimation results (see Table 8).

3.2 | Methodology

The I-S cycle is a typical non-ideal and polar system,[26] and in this system, two acid solutions (ie, the H_2SO_4 and HI solutions) are both easy to be dissociated into ionic compounds via several electrochemical reactions. Therefore, it is essential to integrate some electrochemical reactions into the thermodynamic model of the I-S cycle.[19] As the most versatile electrolyte property method, the

ELECNRTL physical property method of Aspen Plus not only can handle very low and very high concentrations but also can handle aqueous and mixed solvent systems. Therefore, this physical property method is adopted to simulate the Bunsen process and the H_2SO_4 concentration and decomposition process.[26,29] Since the ternary HI-I_2-H_2O mixture has a complex phase behavior, it is very difficult to accurately predict the thermodynamic properties of the HI concentration and decomposition process. Up to now, several physical property methods including NRTL-RK, SR-Polar, ELECNRTL, and so on have been used to simulate the HI-I_2-H_2O system. However, it should be pointed out that each of these physical property methods has its own applicable parameter range, and none of the available physical property models can accurately predict the thermodynamic properties of this complex three-phase mixture under the full parameter range. The development of a complete physical property model requires a large amount of experimental data, and this work exceeds the research scope of our present paper. However, given that the operating conditions of the HI concentration distillation process and the HI decomposition process are significantly different, in this work, the NRTL-RK and SR-Polar physical property methods are respectively used to simulate these two processes.[29] The main equations, application ranges, and limitations of these physical property methods have been summarized in detail in Reference 33.

After determining the physical property methods and component parameters, the software simulation begins, and no error should be reported in the Results Summary when software calculations are completed. Next, the design process of the internal heat exchange network starts and the first step is to collect and organize the heat exchange data (including the inlet and outlet temperatures, heat duty, etc.) of all heat exchangers in the system using Aspen Energy Analyzer. Then, a heat exchange grid diagram can be drawn manually, based on the energy cascade utilization principle (ie, the hot stream with the highest exothermic temperature will be first used to heat the cold stream with the highest endothermic temperature). According to the grid diagram drawn, an initial internal heat exchange network can be designed, and then, the system simulation calculation can be restarted when the operating parameters of all heat exchangers newly added are entered into the software. If there is no error that has been reported in the Results Summary and all heat transfer constraints are satisfied, the software simulation and the entire system design will be both completed. Otherwise, the layout or parameter setting of the designed internal heat exchange network will be modified. The flow chart of the above system design process is presented in Figure 4.

4 | RESULTS AND DISCUSSION

4.1 | Model validation

As mentioned in Section 2.2, the material flow of the Bunsen section in this work is determined based on the study of Guo et al.[28] In this case, the model validation work left for us is to verify the reliability of the simulation results of the H_2SO_4 section and the HI section. Furtherly, since the conversion rates of the chemical decomposition reactions in the H_2SO_4 section and HI section have already been directly specified according to the existing published literature (see Table 1), the model validation of the acid decomposition processes is no longer required. At this time, only the simulation results of the acid concentration/distillation processes need to be verified.

Table 2A,B respectively present the model validation results of the H_2SO_4 distillation process and the HI distillation process. As shown in the two tables, the simulation results we obtained are in good agreement with the results reported in References 24,28, and all relative errors are controlled within 3%. Thus, our simulation model is able to obtain some reliable analysis results.

4.2 | Internal heat exchange network design

As mentioned in Section 1, three sets of different heat transfer constraints corresponding to different temperature zones are imposed in the design process of the internal heat exchange network, which are listed in Table 3. Clearly, the higher the operating temperature of the heat exchanger, the stricter the heat transfer temperature difference constraint (see Table 3). According to the design flow chart of Figure 4 and the heat transfer constraints of Table 3, an I-S system with an internal heat exchange network is developed, as shown in Figure 5. Table 4 gives the detailed material flow data of this system.

From Figure 5, it can be seen that the designed internal heat exchange network consists of nine heat exchangers (ie, IHE1 to IHE9), and most of them are located in the H_2SO_4 concentration and decomposition section and the HI concentration and decomposition section. The detailed heat exchange processes inside these nine internal heat exchangers are shown in Figures 6 to 8 and Table 5.

The IHE1 is located in the Bunsen section and its main task is to heat the cold water fed to the BUNSEN reactor (see Figure 5). Since the top distillate from the H_2SO_4 distillation column (H2SO4DST) needs to be

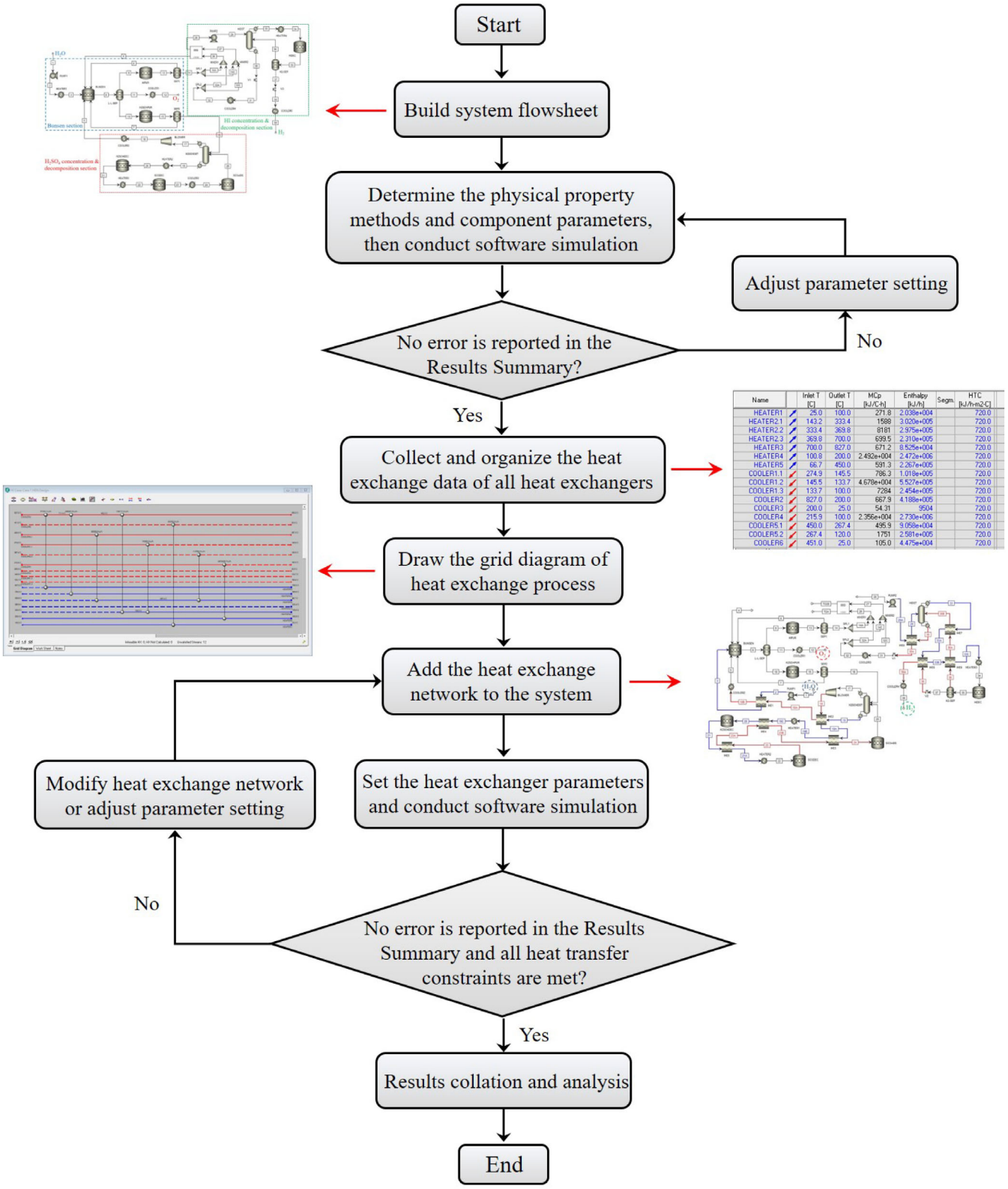

FIGURE 4 Flow chart of the system design process

cooled before entering the BUNSEN reactor (see Figure 2), it is adopted as the hot fluid of IHE1 (see Figure 5). The complete heat exchange process inside IHE1 is presented in Figure 6. It is seen that the heat duty of IHE1 is very small, only about 4.13 kW (see Table 5), and the heat transfer temperature difference (ΔT) is

TABLE 2 Model validation of the (A) H_2SO_4 distillation column (H2SO4DST), (B) HI distillation column (HIDST)

(A) H_2SO_4 distillation column (H2SO4DST)			
Parameters (unit)	**Reference 28**	**Present study**	**Relative errors (%)**
H_2SO_4 mass fraction of the feed H_2SO_4 solution[a] (−)	0.585	0.583	0.34
Distillate ratio of H_2O[b] (−)	0.90	0.91	1.11
H_2SO_4 mass fraction of the bottom product (−)	0.93[c]	0.94	1.08
(B) HI distillation column (HIDST)			
Parameters (unit)	**Reference 24**	**Present study**	**Relative errors (%)**
HI molality of the feed stream, Stream 29 (mol/kg·H_2O)	13.17	13.17	0
HI mole fraction of the top distillate (−)	0.98	1	2.04
HI molality of the bottom product (mol/kg·H_2O)	10.5	10.75	2.38

[a]Only H_2O and H_2SO_4 are counted, excluding O_2 and SO_2.
[b]The ratio of the distillate rate of H_2O to the feed rate of H_2O.
[c]The experimental value is reported to be 0.92 to 0.94.[28]

TABLE 3 Heat transfer constraints in the design process

Temperature zones (°C)	**Minimum terminal heat transfer temperature difference (°C)**	**Minimum pinch point heat transfer temperature difference (°C)**
≥500	30	15
200-500	20	10
≤200	10	5

always large (larger than 90°C). In this situation, the heat transfer process inside IHE1 can proceed smoothly.

There are four internal heat exchangers (ie, IHE2 to IHE5, see Figure 5) located in the H_2SO_4 concentration and decomposition section, and the complete heat exchange processes inside them are shown in Figure 7. The main purpose of setting IHE2, IHE3, and IHE4 is to heat the high-concentration H_2SO_4 solution fed to the H_2SO_4 decomposition reactor (H2SO4DEC), while the IHE5 is used to preheat the H2SO4DEC product (Stream 21) which is sent to the SO_3 decomposition reactor (SO3DEC) for oxygen production, as shown in Figure 5. As mentioned earlier, in this work, the internal heat exchange network is designed based on the energy cascade utilization principle. Given that the SO3DEC product (Stream 23) is the hot stream with the highest exothermic temperature, it should be first used to heat the H2SO4DEC product (Stream 21) with the highest endothermic temperature, and then used to heat the high-concentration H_2SO_4 solution with a moderate endothermic temperature. Therefore, the SO3DEC product (Stream 23) flows sequentially through IHE5, IHE4, and IHE3 as a hot fluid (see Figure 5), and its temperature gradually decreases from 850°C to 200°C, as shown in Figure 7B-D and Table 5. According to the calculation results, a total of about 101 kW of waste heat is recovered using these three internal heat exchangers. Furthermore, by placing IHE2 between the H_2SO_4 distillation column (H2SO4DST) and IHE3 (see Figure 5), about 22.9 kW of waste heat is also recovered from the top distillate of H2SO4DST, as shown in Figure 7A and Table 5.

From Figure 7, it can also be seen that the minimum heat transfer temperature differences of these four internal heat exchangers are respectively equal to 27.94°C, 10.44°C, 20.39°C, and 30.1°C, which are all occurring at the terminal location of the heat exchanger. By comparing these temperature difference data with the minimum values set in Table 3, it can be concluded that all four internal heat exchangers satisfy the current heat transfer constraints.

Similarly, there are also four internal heat exchangers (ie, IHE6 to IHE9, see Figure 5) located in the HI concentration and decomposition section, and the complete heat exchange processes inside them are shown in Figure 8. For IHE6, its main mission is to heat the over-azeotropic HI solution fed to the HIDST, reducing the heat consumption of the HIDST's reboiler. The bottom product of the HIDST is used as the hot fluid, and the detailed heat exchange process inside IHE6 is shown in Figure 8A. It is seen that the heat duty of IHE6 is very large and is equal to about 292.3 kW (see Table 5). This result is considered to be mainly caused by the large material flow of the HI distillation process (see Table 4). Compared with the conversion rate of the H_2SO_4 decomposition reaction, the conversion rate of the HI decomposition reaction is lower, which means that more high-purity HI distillate

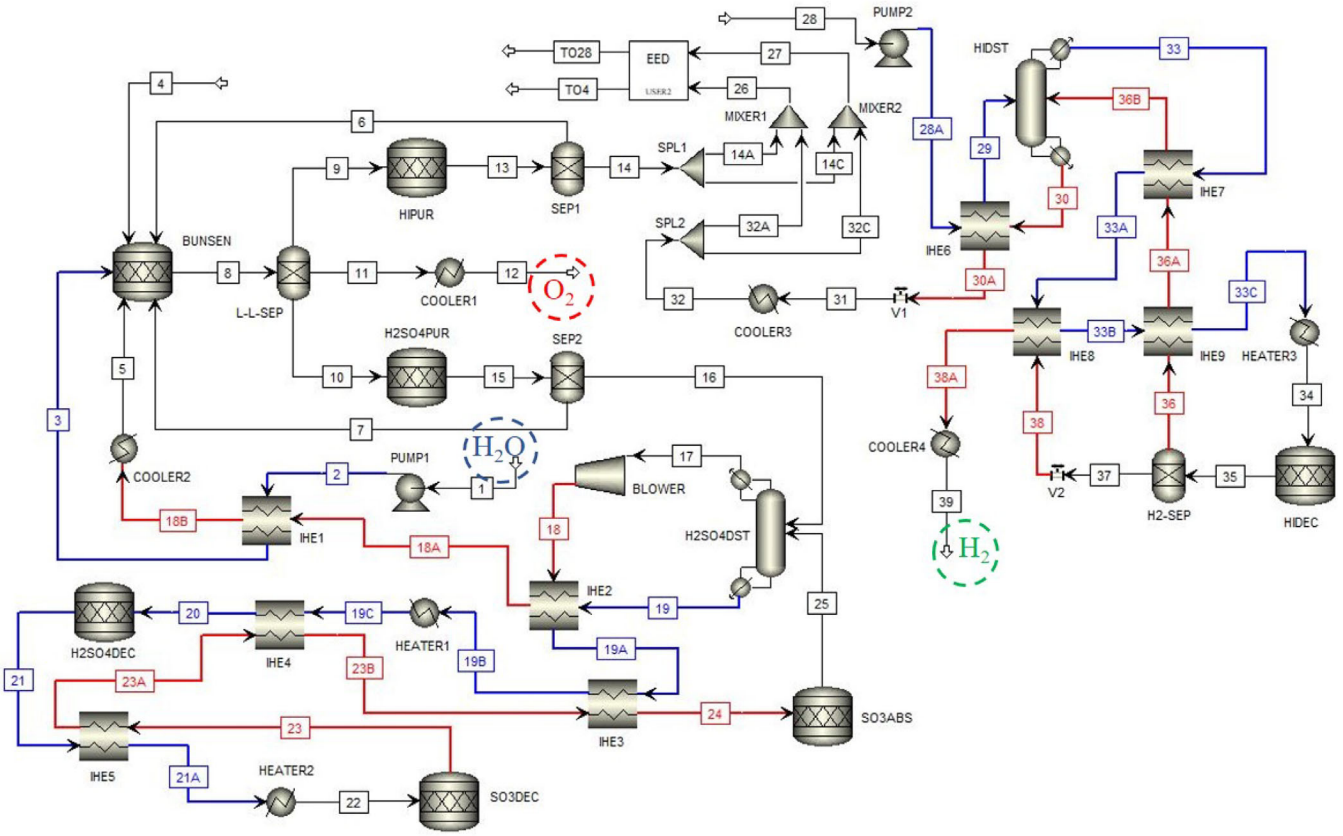

FIGURE 5 Schematic process flowsheet of the designed I-S hydrogen production system with an internal heat exchange network

needs to be sent to the HIDEC for compensating the shortboard of low HI conversion rate. To achieve this objective, the more over-azeotropic HI solution needs to be fed to the HIDST, causing a large material flow in the HI distillation process. In addition, it can also be seen in Figure 8A that the minimum heat transfer temperature difference of IHE6 is equal to 10.01°C, which meets the low-temperature (≤200°C) heat transfer constraint in Table 3.

For IHE7, IHE8, and IHE9, their main task is to heat the high-purity HI fed to the HIDEC, as shown in Figure 5. Due to the good temperature match, the HIDEC product is used as the hot fluid of these three internal heat exchangers. The complete heat exchange processes inside IHE7, IHE8, and IHE9 are presented in Figure 8B-D. It can be seen that when the cold fluid (ie, the high-purity HI) flows sequentially through IHE7, IHE8, and IHE9, it absorbs a total of about 60 kW of waste heat, which improves its temperature from 41.95°C to 421.4°C (see Table 5). Besides, it can also be seen in Figure 8B-D that the minimum heat transfer temperature differences of IHE7, IHE8, and IHE9 are equal to 10.2°C, 21.52°C, and 20°C, respectively. For IHE8 and IHE9, their minimum heat transfer temperature differences are both appearing at the terminal location of the heat exchanger, but for IHE7, that is occurring inside the heat exchanger (at this time, the pinch point temperature difference constraint should be considered, which emphasizes the necessity of analyzing the complete heat transfer process inside the heat exchanger at the design stage). Anyway, by comparing these temperature difference values with the minimum values set in Table 3, it can be concluded that all three internal heat exchangers satisfy the current heat transfer constraints.

4.3 | Energy consumption and thermal efficiency analysis of the I-S system

In this work, the energy consumption of the Bunsen section is omitted due to its small value (almost 0[24]). The detailed energy consumption data of the I-S system with an internal heat exchange network (hydrogen yield of 1 mol/s) are presented in Table 6 and Figure 9. It is calculated that for the proposed I-S system with an internal heat exchange network, producing 1 mol of hydrogen requires consuming about 1046.5 kJ of heat and about 151.4 kJ of electricity, if no other waste heat recovery measures are used further. Assuming the electricity generation efficiency of 45%,[26] the total heat demand for

TABLE 4 Material flow data of the designed I-S hydrogen production system with an internal heat exchange network

			Molar flow rate (mol/s)							
Stream No.	***T* (K)**	***p* (MPa)**	**H_2O**	**H_2SO_4**	**HI**	**I_2**	**SO_2**	**SO_3**	**O_2**	**H_2**
1	298.15	0.101	1	0	0	0	0	0	0	0
2	298.17	0.5	1	0	0	0	0	0	0	0
3	353	0.5	1	0	0	0	0	0	0	0
4	353	0.5	30.841	0	2.546	8.545	0	0	0	0
5	353	0.5	4.556	0	0	0	1	0	0.5	0
6	353	0.5	0	0	0	0	0.565	0	0	0
7	353	0.5	0.944	0	0	0.159	0.091	0	0	0
8	353	0.5	34.028	1.656	5.859	7.048	0	0	0.5	0
9	353	0.5	29.71	0.565	5.677	6.98	0	0	0	0
10	353	0.5	4.318	1.091	0.182	0.068	0	0	0	0
11	353	0.5	0	0	0	0	0	0	0.5	0
12	313	0.5	0	0	0	0	0	0	0.5	0
13	353	0.5	30.841	0	4.546	7.545	0.565	0	0	0
14	353	0.5	30.841	0	4.546	7.545	0	0	0	0
15	353	0.5	4.5	1	0	0.159	0.091	0	0	0
16	353	0.5	3.556	1	0	0	0	0	0	0
17	365.54	0.101	4.556	0	0	0	1	0	0.5	0
18	546.71	0.5	4.556	0	0	0	1	0	0.5	0
18A	445.15	0.5	4.556	0	0	0	1	0	0.5	0
18B	426.58	0.5	4.556	0	0	0	1	0	0.5	0
19	417.21	0.101	0.439	1.282	0	0	0	0	0	0
19A	462.71	0.101	0.439	1.282	0	0	0	0	0	0
19B	574.75	0.101	0.439	1.282	0	0	0	0	0	0
19C	698.15	0.101	0.439	1.282	0	0	0	0	0	0
20	773.15	0.101	0.439	1.282	0	0	0	0	0	0
21	773.15	0.101	1.721	0	0	0	0	1.282	0	0
21A	1088.15	0.101	1.721	0	0	0	0	1.282	0	0
22	1123.15	0.101	1.721	0	0	0	0	1.282	0	0
23	1123.15	0.101	1.721	0	0	0	1	0.282	0.5	0
23A	803.26	0.101	1.721	0	0	0	1	0.282	0.5	0
23B	718.54	0.101	1.721	0	0	0	1	0.282	0.5	0
24	473.15	0.101	1.721	0	0	0	1	0.282	0.5	0
25	473.15	0.101	1.439	0.282	0	0	1	0	0.5	0
26	354.23	0.5	33.513	0	5.229	7.21	0	0	0	0
27	353.13	0.5	43.408	0	8.237	4.335	0	0	0	0
28	353	0.5	46.08	0	10.92	3	0	0	0	0
28A	353.18	1.17	46.08	0	10.92	3	0	0	0	0
29	412.15	1.17	46.08	0	10.92	3	0	0	0	0
30	422.23	1.17	46.08	0	8.92	4	0	0	0	0
30A	371.46	1.17	46.08	0	8.92	4	0	0	0	0
31	371.53	0.5	46.08	0	8.92	4	0	0	0	0
32	353	0.5	46.08	0	8.92	4	0	0	0	0

(Continues)

TABLE 4 (Continued)

Stream No.	T (K)	p (MPa)	Molar flow rate (mol/s)							
			H_2O	H_2SO_4	HI	I_2	SO_2	SO_3	O_2	H_2
33	315.10	1.17	0	0	5	0	0	0	0	0
33A	633.15	1.17	0	0	5	0	0	0	0	0
33B	646.15	1.17	0	0	5	0	0	0	0	0
33C	694.55	1.17	0	0	5	0	0	0	0	0
34	723	1.17	0	0	5	0	0	0	0	0
35	723	1.17	0	0	3	1	0	0	0	1
36	723	1.17	0	0	3	1	0	0	0	0
36A	666.15	1.17	0	0	3	1	0	0	0	0
36B	468.42	1.17	0	0	3	1	0	0	0	0
37	723	1.17	0	0	0	0	0	0	0	1
38	723.63	0.101	0	0	0	0	0	0	0	1
38A	654.67	0.101	0	0	0	0	0	0	0	1
39	313	0.101	0	0	0	0	0	0	0	1

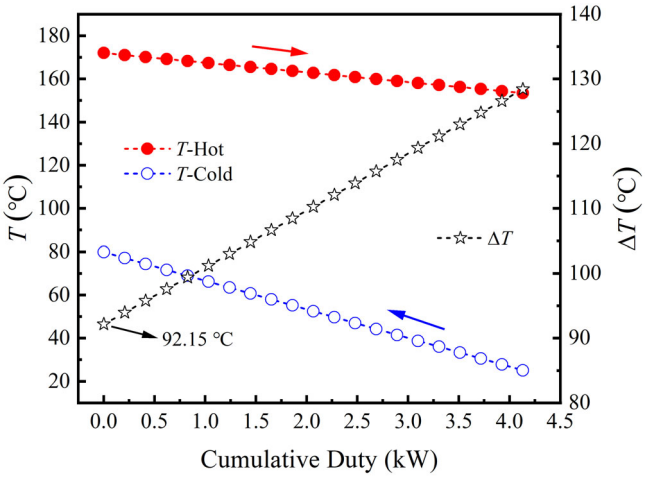

FIGURE 6 Heat exchange process of IHE1

producing 1 mol of hydrogen is calculated to be about 1382.9 kJ. From Figure 9, it can be seen that the biggest energy consumption of the I-S system comes from the reboiler of H2SO4DST, which accounts for about 27.4% of the system's total energy consumption. Besides, about 23.5% and 17.8% of the system's total energy consumption are occupied by the reboiler of HIDST and the EED cell, respectively. In short, it can be concluded that more than half of the system energy consumption (ie, 27.4% + 23.5% = 50.9%) is occupied by two distillation columns and more than 40% of the system energy consumption (ie, 23.5% + 17.8% = 41.3%) is used by the HI concentration and distillation process.

For the I-S system without an internal heat exchange network (see Figure 2), it is calculated that producing 1 mol of hydrogen requires consuming about 1468.5 kJ of heat and about 151.4 kJ of electricity, which means that a total of about 1804.9 kJ of heat is required. Therefore, it can be concluded that with the current internal heat exchange network, about 422 kJ of waste heat can be effectively recovered per 1 mol of hydrogen produced. Furthermore, according to Equation (9), the thermal efficiencies of the I-S systems with and without the internal heat exchange network are calculated to be about 20.7% and 15.8%, respectively, which means that an efficiency improvement of around 4.9% is achieved using the present internal heat exchange network.

Given that the distillation processes of two acid solutions (or the reboilers of two distillation columns, see Figure 9A) will consume a large amount of low-grade thermal energy, in some previous studies, the heat released by the condenser of the distillation column is assumed to be completely recovered for supplying part of the distillation heat.[12] In this work, it is calculated that the heat released by the condensers of H2SO4DST and HIDST is respectively equal to about 249.6 and 252.6 kJ. If all this heat is effectively recovered, the total heat demand in Table 6 will become 880.7 kJ, and the thermal efficiency of the system will be improved to about 32.5% (at this time, an efficiency improvement of about 11.8% is achieved). Thus, it can be concluded that the waste heat recovery from the distillation processes is essential to improve the thermal efficiency of the I-S system. In addition, according to References 7, 31, electric conversion efficiency of 15% can be considered to recover the remaining waste heat with temperatures higher than 313 K further (note that only the waste heat released by

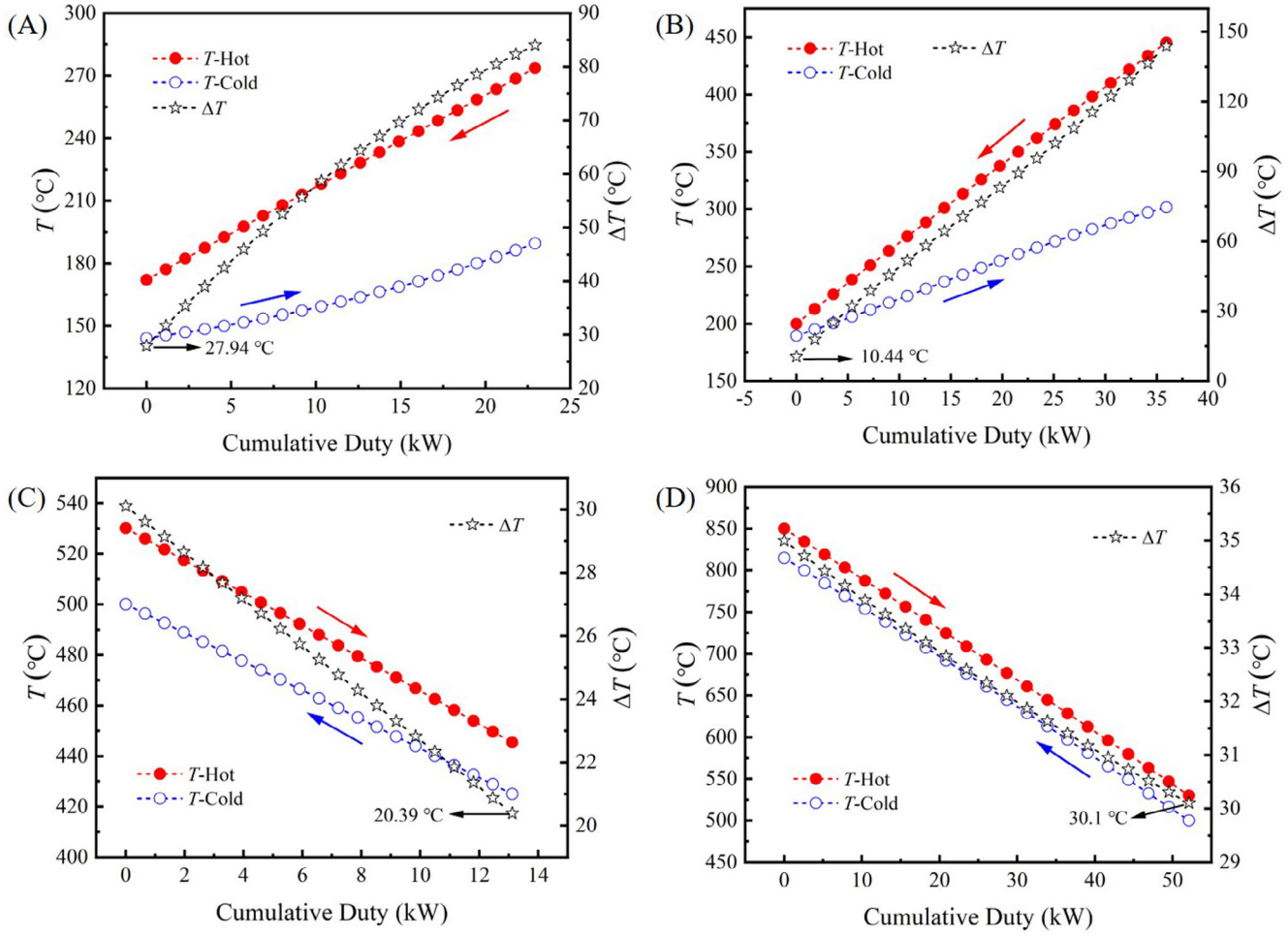

FIGURE 7 Heat exchange processes of (A) IHE2, (B) IHE3, (C) IHE4, and (D) IHE5

the heat exchanger is recyclable[26]). Thus, about 46 kJ of electricity can be generated by recovering this part of waste heat, and the thermal efficiency of the I-S system can be further improved to around 36.7%. Assuming that all recyclable waste heat (not including the heat released from the chemical reactor) is recovered at 100% efficiency, an ideal maximum thermal efficiency of about 49.8% can be achieved by the proposed I-S system. In summary, the thermal efficiency estimation value is strongly dependent on the adopted system assumptions. The above analysis results of the system's energy consumption and thermal efficiency are summarized in Table 7.

Up to now, there are some studies on the thermal efficiency analysis of the I-S system that have been conducted, as summarized in Table 8. It should be emphasized that all the results listed in Table 8 are obtained based on theoretical calculation or software simulation. It can be seen from the table that the process flowsheet of conventional Bunsen reaction accompanied by concentration, distillation, and decomposition of H_2SO_4 and HI is adopted in most studies, and the main difference among these studies lies in the HI concentration and distillation method used (such as the EED and distillation method, reactive distillation method, etc.). It is worth noting that several new processes including the electrochemical Bunsen process and HI electrolysis process are also used in some studies, such as References 7, 17, 26. Besides, it can also be seen from Table 8 that the thermal efficiency estimation results of different studies are significantly different, and in general, the thermal efficiency estimation value is in the range of 15.3% to 57% (our estimation results are covered by this range). In terms of the thermal efficiency of the system, the I-S system we proposed can compete with the systems proposed in References 7, 35, 37.

5 | CONCLUSION AND OUTLOOK

An I-S thermochemical cycle-based hydrogen production system with an internal heat exchange network is

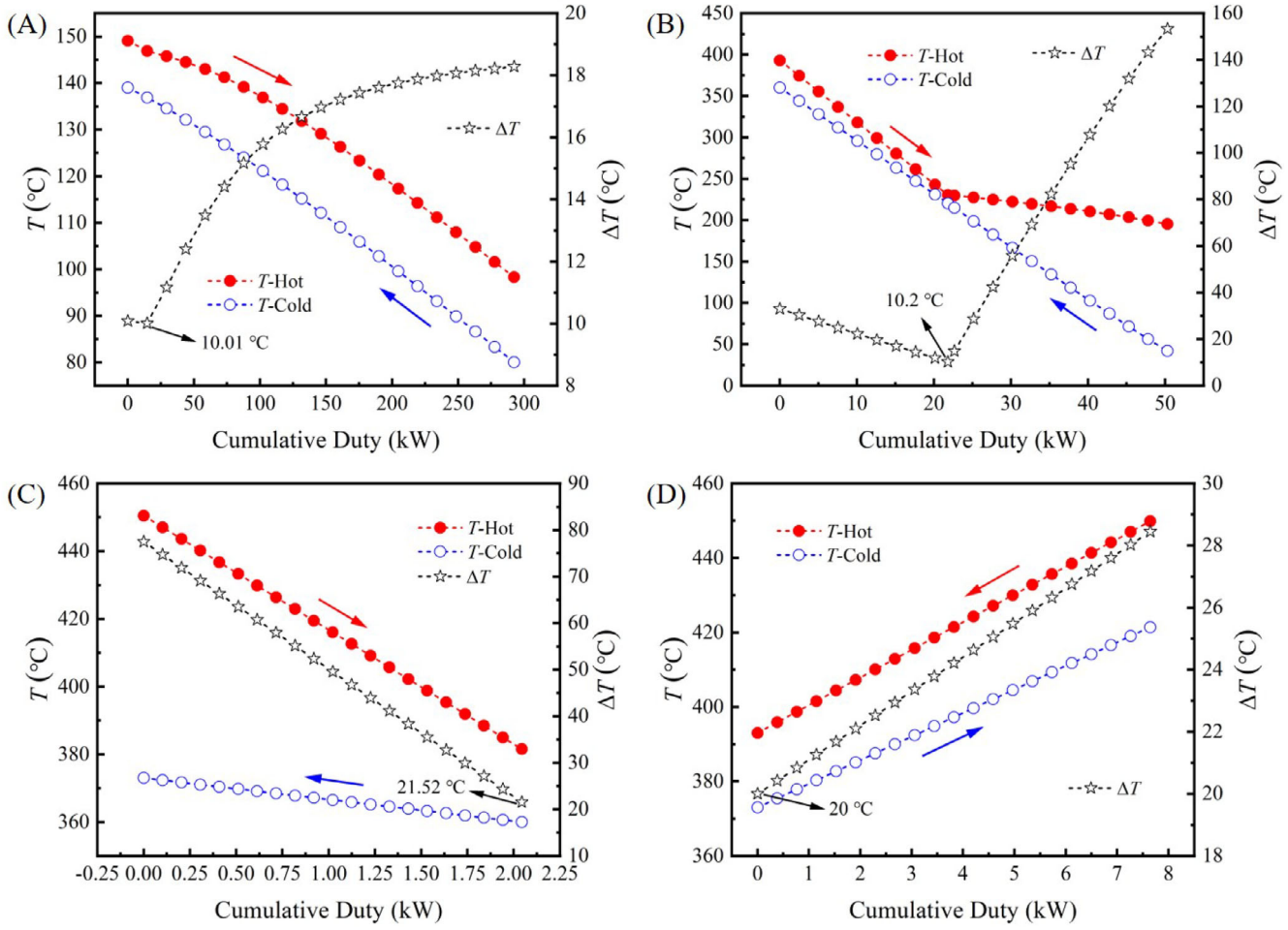

FIGURE 8 Heat exchange processes of (A) IHE6, (B) IHE7, (C) IHE8, and (D) IHE9

TABLE 5 Detailed operating data of the designed internal heat exchange network

Components	Heat duty (kW)	Inlet temperature of hot fluid (°C)	Outlet temperature of hot fluid (°C)	Inlet temperature of cold fluid (°C)	Outlet temperature of cold fluid (°C)
IHE1	4.13	172	153.43	25.02	79.85
IHE2	22.93	273.56	172	144.06	189.56
IHE3	35.92	445.39	200	189.56	301.6
IHE4	13.12	530.11	445.39	425	500
IHE5	52.12	850	530.11	500	815
IHE6	292.32	149.08	98.31	80.03	139
IHE7	50.31	393	195.27	41.95	360
IHE8	2.04	450.48	381.52	360	373
IHE9	7.64	449.85	393	373	421.4

proposed and studied in this paper, based on Aspen Plus software. The internal heat exchange network is designed by following the energy cascade utilization principle, and three sets of different heat transfer constraints corresponding to different temperature zones are imposed in the design process. The designed internal heat exchange network consists of nine heat exchangers, and the heat transfer processes inside these nine heat

TABLE 6 Energy consumption of the I-S system with an internal heat exchange network

Sections	Heat demand (kJ)	Electricity demand (kJ)	Heat required for electricity[a] (kJ)	Total heat demand (kJ)
Bunsen section	-	-	-	-
H_2SO_4 section	704.2	39.2	87.1	791.3
HI section	342.3	112.2	249.3	591.6
Whole system	1046.5	151.4	336.4	1382.9

[a]The electricity generation efficiency is set to 45%.[26]

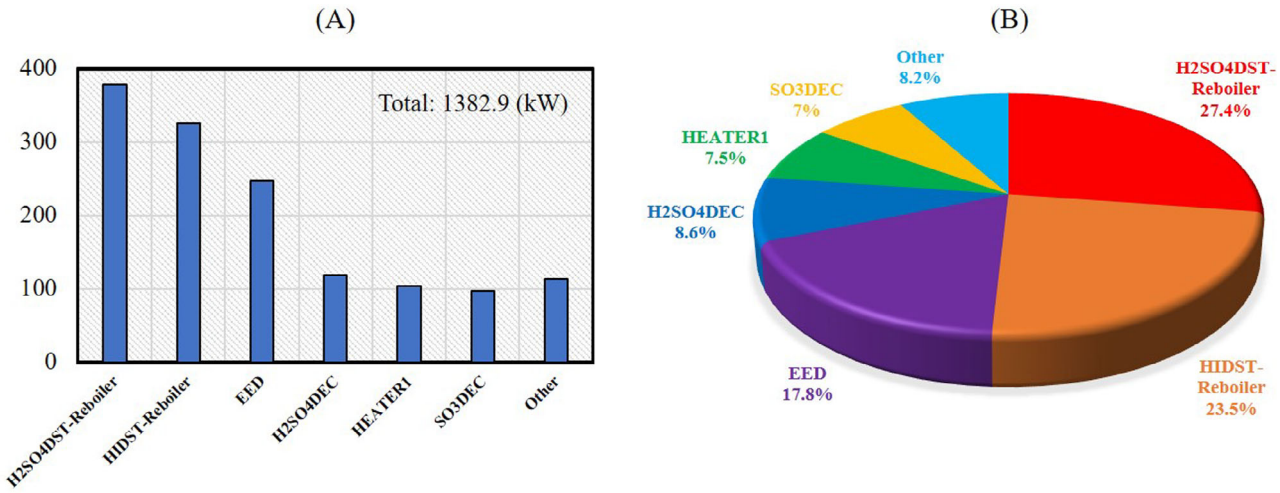

FIGURE 9 Energy consumption distribution of the I-S system with an internal heat exchange network

TABLE 7 Several different analysis results in the I-S system's energy consumption and thermal efficiency

System (adopted waste heat recovery measures)	Heat demand (kJ)	Electricity demand (kJ)	Total heat demand (kJ)	Thermal efficiency (%)
Original I-S system (without waste heat recovery)	1468.5	151.4	1804.9	15.8
Improved I-S system (internal heat exchange network)	1046.5	151.4	1382.9	20.7
Improved I-S system (internal heat exchange network, distillation heat recovery)	544.3	151.4	880.7	32.5
Improved I-S system (internal heat exchange network, distillation heat recovery, electricity recovery)	544.3	105.4	778.5	36.7
Ideal I-S system (all recyclable waste heat is recovered at 100% efficiency)	237.8	151.4	574.2	49.8

TABLE 8 Summary of the thermal efficiency estimation results of the I-S system

Researchers (Year)	Main process characteristics			Efficiency range (%)	Best estimate (%)
	Bunsen section	H_2SO_4 section	HI section		
Kasahara et al[30] (2003)	Conventional Bunsen reaction	Multi-effect evaporation for concentrating H_2SO_4	EED and distillation for concentrating HI	-	56.8
Goldstein et al[12] (2005)	Conventional Bunsen reaction	Multi-stage distillation for concentrating H_2SO_4	Reactive distillation for concentrating HI	≤51	33-36
Kasahara et al[14] (2007)	Conventional Bunsen reaction	Multi-effect evaporation for concentrating H_2SO_4	EED and distillation for concentrating HI	≤57	34
Lee et al[34] (2009)	Optimized Bunsen reaction for producing over-azeotropic HI solution	Flash evaporation for concentrating H_2SO_4	Flash evaporation for concentrating HI	-	47-48
Liberatore et al[35] (2012)	Conventional Bunsen reaction	Multi-stage flash evaporation for concentrating H_2SO_4	Reactive distillation for concentrating HI	-	21-34
Shin et al[36] (2012)	Conventional Bunsen reaction	Multi-stage distillation for concentrating H_2SO_4	EED and distillation for concentrating HI	-	39.4
Ying et al[17] (2017)	Electrochemical Bunsen reaction for producing over-azeotropic HI solution	Flash evaporation for concentrating H_2SO_4	Flash evaporation for concentrating HI	≤50	42
Rodríguez et al[37] (2018)	Conventional Bunsen reaction	Multi-stage distillation for concentrating H_2SO_4	Reactive distillation for concentrating HI	-	22.56
Kasahara et al[24] (2018)	Conventional Bunsen reaction	Flash evaporation for concentrating H_2SO_4	EED and distillation for concentrating HI	-	50.2
Ying et al[26] (2020)	Conventional Bunsen reaction	Multi-stage distillation for concentrating H_2SO_4	HI electrolysis for H_2 production	25-42	33.3
Ying et al[7] (2021)	Conventional Bunsen reaction	Multi-stage distillation for concentrating H_2SO_4	HI electrolysis for H_2 production	15.3-31	19.2
Wang et al (2022) (this work)	Conventional Bunsen reaction	Multi-stage distillation for concentrating H_2SO_4	EED and distillation for concentrating HI	15.8-49.8	20.7-36.7

exchangers are analyzed in detail. Finally, the energy consumption and thermal efficiency of the I-S system under different operating conditions are calculated.

The main results show that for the I-S system with an internal heat exchange network, the biggest energy consumption is caused by the H_2SO_4 distillation column (H2SO4DST), followed by the HIDST and the EED cell. More than half of the system energy consumption is occupied by two distillation columns and more than 40% of the system energy consumption is used by the HI concentration and distillation process. With the current internal heat exchange network, about 422 kJ of waste heat (for 1 mol of hydrogen production) can be effectively recovered, which ultimately brings an efficiency increase of around 4.9%. In addition, it is also found that an efficiency improvement of about 11.8% can be achieved when the waste heat from the condensers of two distillation columns is completely recovered. In general, the thermal efficiency of the proposed I-S system is estimated to be in the range of 15.8% to 49.8%, which is strongly dependent on the adopted system assumptions. Using several common waste heat recovery methods, a promising thermal efficiency of approximately 36.7% can be achieved by the system.

It should be pointed out that in this work, the internal heat exchange network is designed only from the perspective of thermodynamic feasibility while the economic performance is not considered, which is the main

research limitation of this paper. Given that several internal heat exchangers (such as IHE1, IHE8, and IHE9) have relatively small heat duties (see Table 5) but lead to additional investment and maintenance costs, it will be merited to further conduct a study on the tradeoff between the thermodynamic benefits and the economic costs (as one of our future studies). Anyway, this paper presents a new I-S process flowsheet and a new design idea for the internal heat exchange network. These new elements enrich the existing research on the I-S cycle and also promote further applications of the I-S cycle.

ACKNOWLEDGEMENT

Qi Wang greatly appreciates the China Scholarship Council (CSC) for the financial support of this research (Grant No. 202006280024). Open Access funding enabled and organized by Projekt DEAL.

CONFLICT OF INTERESTS

The authors declare no conflicts of interest.

DATA AVAILABILITY STATEMENT

Data available on request from the authors.

ORCID

Qi Wang https://orcid.org/0000-0001-6656-2899

REFERENCES

1. Hydrogen scaling up. A sustainable pathway for the global energy transition, Hydrogen Council. 2017.
2. El-Emam RS, Ozcan H, Zamfirescu C. Updates on promising thermochemical cycles for clean hydrogen production using nuclear energy. *J Clean Prod*. 2020;262:121424.
3. Şahin S, Şahin HM. Generation-IV reactors and nuclear hydrogen production. *Int J Hydrog Energy*. 2021;46(57):28936-28948.
4. Vitart X, Le Duigou A, Carles P. Hydrogen production using the sulfur-iodine cycle coupled to a VHTR: an overview. *Energy Convers Manag*. 2006;47(17):2740-2747.
5. Ewan BCR, Allen RWK. A figure of merit assessment of the routes to hydrogen. *Int J Hydrog Energy*. 2005;30(8):809-819.
6. Wang Q, Liu C, Luo R, Li D, Macián-Juan R. Thermodynamic analysis and optimization of the combined supercritical carbon dioxide Brayton cycle and organic Rankine cycle-based nuclear hydrogen production system. *Int J Energy Res*. 2022;46(2):832-859.
7. Ying Z, Yang JY, Zheng XY, Wang Y, Dou B. Energy and exergy analyses of a novel sulfur–iodine cycle assembled with HI–I_2–H_2O electrolysis for hydrogen production. *Int J Hydrog Energy*. 2021;46(45):23139-23148.
8. Farsi A, Dincer I, Naterer GF. Review and evaluation of clean hydrogen production by the copper–chlorine thermochemical cycle. *J Clean Prod*. 2020;276:123833.
9. Yilmaz F, Selbaş R. Thermodynamic performance assessment of solar based sulfur-iodine thermochemical cycle for hydrogen generation. *Energy*. 2017;140(Part 1):520-529.
10. Wang Q, Liu C, Luo R, Li X, Li D, Macián-Juan R. Thermo-economic analysis and optimization of the very high temperature gas-cooled reactor-based nuclear hydrogen production system using copper-chlorine cycle. *Int J Hydrog Energy*. 2021;46(62):31563-31585.
11. Qu X, Zhao G, Wang J. Thermodynamic evaluation of hydrogen and electricity cogeneration coupled with very high temperature gas-cooled reactors. *Int J Hydrog Energy*. 2021;46(57):29065-29075.
12. Goldstein S, Borgard JM, Vitart X. Upper bound and best estimate of the efficiency of the iodine Sulphur cycle. *Int J Hydrog Energy*. 2005;30(6):619-626.
13. O'Keefe D, Allen C, Besenbruch G, et al. Preliminary results from bench-scale testing of a sulfur-iodine thermochemical water-splitting cycle. *Int J Hydrog Energy*. 1982;7(5):381-392.
14. Kasahara S, Kubo S, Hino R, Onuki K, Nomura M, Nakao SI. Flowsheet study of the thermochemical water-splitting iodine-sulfur process for effective hydrogen production. *Int J Hydrog Energy*. 2007;32(4):489-496.
15. Guo HF, Zhang P, Bai Y, Wang LJ, Chen SZ, Xu JM. Continuous purification of H_2SO_4 and HI phases by packed column in IS process. *Int J Hydrog Energy*. 2010;35(7):2836-2839.
16. Guo HF, Zhang P, Chen SZ, Wang L, Xu J. Comparison of various circuit designs in the HI decomposition section of the iodine–sulfur process. *Int J Hydrog Energy*. 2012;37(17):12097-12104.
17. Ying Z, Zheng XY, Zhang Y, Cui G. Development of a novel flowsheet for sulfur–iodine cycle based on the electrochemical Bunsen reaction for hydrogen production. *Int J Hydrog Energy*. 2017;42(43):26586-26596.
18. Zhu QQ, Zhang YW, Ying Z, Zhou JH, Wang ZH, Cen KF. Occurrence of the Bunsen side reaction in the sulfur-iodine thermochemical cycle for hydrogen production. *J Zhejiang Univ-Sci A (Appl Phys Eng)*. 2013;14(4):300-306.
19. Park J, Cho JH, Jung H, Jung KD, Kumar S, Moon I. Simulation and experimental study on the sulfuric acid decomposition process of SI cycle for hydrogen production. *Int J Hydrog Energy*. 2013;38(14):5507-5516.
20. Gao Q, Sun Q, Zhang P, Peng W, Chen S. Sulfuric acid decomposition in the iodine–sulfur cycle using heat from a very high temperature gas-cooled reactor. *Int J Hydrog Energy*. 2021;46(57):28969-28979.
21. Guo HF, Kasahara S, Onuki K, Zhang P, Xu J. Simulation study on the distillation of hyper-pseudoazeotropic HI-I_2-H_2O mixture. *Ind Eng Chem Res*. 2011;50(20):11644-11656.
22. Yamawaki M, Nishihara T, Inagaki Y, et al. Application of nuclear energy for environmentally friendly hydrogen generation. *Int J Hydrog Energy*. 2007;32(14):2719-2725.
23. Zhang P, Wang L, Chen SG, et al. Progress of nuclear hydrogen production through the iodine-sulfur process in China. *Renew Sust Energ Rev*. 2018;81(Part 2):1802-1812.
24. Kasahara S, Imai Y, Suzuki K, Iwatsuki J, Terada A, Yan XL. Conceptual design of the iodine-sulfur process flowsheet with more than 50% thermal efficiency for hydrogen production. *Nucl Eng Des*. 2018;329:213-222.
25. Park JK, Ifaei P, Ba-Alawi AH, Safder U, Yoo CK. Hydrogen production through the sulfur–iodine cycle using a steam boiler heat source for risk and techno-socio-economic cost (RSTEC) reduction. *Int J Hydrog Energy*. 2020;45(28):14578-14593.

26. Ying Z, Wang YB, Zheng XY, Geng Z, Dou B, Cui G. Experimental study and development of an improved sulfur-iodine cycle integrated with HI electrolysis for hydrogen production. *Int J Hydrog Energy*. 2020;45(24):13176-13188.
27. Juárez-Martínez LC, Espinosa-Paredes G, Vázquez-Rodríguez A, Romero-Paredes H. Energy optimization of a sulfur–iodine thermochemical nuclear hydrogen production cycle. *Nucl Eng Technol*. 2021;53(6):2066-2073.
28. Guo H, Zhang P, Chen S, Wang L, Xu J. Modeling and validation of the iodine-sulfur hydrogen production process. *AICHE J*. 2014;60(2):546-558.
29. Wang Z, Yang J, Zhang Y, et al. Simulation of hydrogen production by sulfur-iodine thermo-chemical cycle process. *Taiyangneng Xuebao/Acta Energ Sol Sin*. 2011;32(6):802-807.
30. Kasahara S, Hwang GJ, Nakajima H, Choi HS, Onuki K, Nomura M. Effects of process parameters of the IS process on total thermal efficiency to produce hydrogen from water. *J Chem Eng Jpn*. 2003;36(7):887-899.
31. Wang Q, Liu C, Li D, Macián-Juan R. Optimization and comparison of two improved very high temperature gas-cooled reactor-based hydrogen and electricity cogeneration systems using iodine-sulfur cycle. *Int J Hydrog Energy*. 2022; (In Press). https://doi.org/10.1016/j.ijhydene.2022.02.237
32. Tanaka N, Onuki K. Equilibrium potential across cation exchange membrane in HI–I_2–H_2O solution. *J Membr Sci*. 2010;357(1–2):73-79.
33. Aspen Technology, Inc. Aspen physical property system: physical property methods. Version Number: V7.3, Aspen Technology, Inc., Burlington, MA, 2011.
34. Lee BJ, No HC, Yoon HJ, et al. Development of a flowsheet for iodine-sulfur thermo-chemical cycle based on optimized Bunsen reaction. *Int J Hydrog Energy*. 2009;34(5):2133-2143.
35. Liberatore R, Lanchi M, Giaconia A, Tarquini P. Energy and economic assessment of an industrial plant for the hydrogen production by water-splitting through the sulfur-iodine thermochemical cycle powered by concentrated solar energy. *Int J Hydrog Energy*. 2012;37(12):9550-9565.
36. Shin Y, Lee K, Kim Y, Chang J, Cho W, Bae K. A sulfur-iodine flowsheet using precipitation, electrodialysis, and membrane separation to produce hydrogen. *Int J Hydrog Energy*. 2012;37(21):16604-16614.
37. Rodríguez DG, de Oliveira B, Lira CA, García Parra LR, et al. Computational model of a sulfur-iodine thermochemical water splitting system coupled to a VHTR for nuclear hydrogen production. *Energy*. 2018;147:1165-1176.

How to cite this article: Wang Q, Macián-Juan R. Design and analysis of an iodine-sulfur thermochemical cycle-based hydrogen production system with an internal heat exchange network. *Int J Energy Res*. 2022;46(9):11849-11866. doi:10.1002/er.7951